



PAPER

OPEN ACCESS

RECEIVED
6 September 2024REVISED
21 October 2024ACCEPTED FOR PUBLICATION
13 November 2024PUBLISHED
24 December 2024

Original content from
this work may be used
under the terms of the
[Creative Commons
Attribution 4.0 licence](#).

Any further distribution
of this work must
maintain attribution to
the author(s) and the title
of the work, journal
citation and DOI.



Spatially fractionated radiotherapy with very high energy electron pencil beam scanning

Jade Fischer^{1,*} , Alexander Hart¹ , Nicole Bedriová² , Deae-eddine Krim¹ , Nathan Clements¹ , Joseph Bateman³ , Pierre Korysko³ , Wilfrid Farabolini⁴, Vilde Rieker⁵, Roberto Corsini⁴, Manjit Dosanjh¹  and Magdalena Bazalova-Carter¹ 

¹ Department of Physics and Astronomy, University of Victoria, Victoria, Canada

² Department of Physics, University of Zilina, Zilina, Slovakia

³ Department of Physics, University of Oxford, Oxford, United Kingdom

⁴ CERN, Geneva, Switzerland

⁵ Department of Physics, University of Oslo, Oslo, Norway

* Author to whom any correspondence should be addressed.

E-mail: JadeFischer@uvic.ca

Keywords: radiotherapy, very-high energy electrons, spatially fractionated radiation therapy, Monte Carlo simulations, film dosimetry, treatment planning

Abstract

Objective. To evaluate spatially fractionated radiation therapy (SFRT) for very-high-energy electrons (VHEEs) delivered with pencil beam scanning. **Approach.** Radiochromic film was irradiated at the CERN linear electron accelerator for research using 194 MeV electrons with a step-and-shoot technique, moving films within a water tank. Peak-to-valley dose ratios (PVDRs), depths of convergence (PVDR ≤ 1.1), peak doses, and valley doses assessed SFRT dose distribution quality. A Monte Carlo (MC) model of the pencil beams was developed using TOPAS and applied to a five-beam VHEE SFRT treatment for a canine glioma patient, compared to a clinical 6 MV VMAT plan. The plans were evaluated based on dose-volume histograms, mean dose, and maximum dose to the planning target volume (PTV) and organs at risks (OARs). **Main results.** Experimental PVDR values were maximized at 15.5 ± 0.1 at 12 mm depth for 5 mm spot spacing. A DOC of 76.5, 70.7, and 56.6 mm was found for 5, 4, and 3 mm beamlet spacings, respectively. MC simulations and experiments showed good agreement, with maximum relative dose differences of 2% in percentage depth dose curves and less than 3% in beam profiles. Simulated PVDR values reached 180 ± 4 , potentially achievable with reduced leakage dose. VHEE SFRT plans for the canine glioma patient showed a decrease in mean dose ($>16\%$) to OARs while increasing the PTV mean dose by up to 15%. Lowering beam energy enhanced PTV dose homogeneity and reduced OAR maximum doses. **Significance.** The presented work demonstrates that pencil beam scanning SFRT with VHEEs could treat deep-seated tumors such as head and neck cancer or lung lesions, though small beam size and leakage dose may limit the achievable PVDR.

1. Introduction

Radiation therapy (RT) is recommended for nearly half of all cancer patients (Delaney *et al* 2005), however the risk of toxicity to the organs surrounding the tumor remains a dose-limiting factor in radiotherapy. Substantial advancements have been made to improve the conformity (CI) of dose distributions and minimize entrance dose through techniques such as volumetric modulated arc therapy (VMAT) (Otto 2008) and particle therapy (Kiseleva *et al* 2022). Recently, there has been significant interest towards techniques which show normal tissue sparing, even in the presence of high doses.

Spatially fractionated RT (SFRT) is one such technique which delivers a heterogeneous dose distribution consisting of alternating high and low dose regions (Billena and Khan 2019). SFRT has exhibited the potential to present low toxicity without compromising treatment efficacy (Slatkin *et al* 1992, Mohiuddin

et al 1999, Peñagaricano *et al* 2009, Prezado *et al* 2017). Clinical applications for SFRT have been found in bulky tumors, specifically for head and neck patients (Neuner *et al* 2012, Choi *et al* 2019), and there are promising results for sarcoma patient (Snider *et al* 2020, Ahmed *et al* 2024). The SFRT approach has demonstrated its effectiveness in addressing radio resistant tumors (Gholami *et al* 2016). The radiobiological mechanism behind normal tissue sparing in SFRT is not yet understood, but several radiobiological effects have been proposed as an explanation. Current theories suggest that SFRT is able to maintain a therapeutic benefit due to differential vascular damage, abscopal effects, and the bystander effect (Asur *et al* 2015, Tubin *et al* 2019, Yan *et al* 2020). SFRT has been categorized into a variety of forms which vary primarily based on beamlet size. GRID therapy uses a physical collimator to create beamlets ranging from 0.5 to 2 cm, forming a characteristic SFRT grid-like pattern. In contrast, microbeam radiotherapy employs much smaller beamlets of 25–100 μm delivered at high dose rates to prevent smearing, while minibeam radiotherapy utilizes slightly larger beamlets in the range of 0.5–1 mm (Fukunaga *et al* 2021). Several dosimetric parameters have been identified which may be predictive of normal tissue sparing, namely the peak to valley dose ratio (PVDR), beamlet spacing and beamlet size (Anderson *et al* 2012, Smyth *et al* 2016). The PVDR is the ratio of the dose in the peak to the dose in the valley and the beamlet spacing is the center-to-center distance between peaks. More recent studies indicated that the valley dose is the key parameter defining normal tissue sparing (Rivera *et al* 2020, Fernandez-Palomo *et al* 2022). Extending the PVDR, another relevant metric is the depth of convergence (DOC) which measures the depth at which the PVDR < 1.1 and the characteristic SFRT pattern is no longer visible. At such depths the normal tissue sparing of SFRT would no longer be present and the DOC then defines the limitations for what lesions are treatable with SFRT (Clements *et al* 2023).

Very high energy electrons (VHEEs) are a promising new modality that offers unique physical and dosimetric properties that are well suited for the delivery of SFRT. VHEE beams exhibit lower lateral scatter than photon beams (DesRosiers *et al* 2000) and are more insensitive to inhomogeneities compared to other charged particle therapies (Lagzda *et al* 2020), both of which contribute to higher PVDRs. A Monte Carlo (MC) simulation study investigating 250 MeV VHEE SFRT demonstrated that PVDRs greater than 30 could be achieved at the surface using a tungsten collimator with $0.5 \times 0.5 \text{ mm}^2$ channels (Clements *et al* 2023). VHEE sources have the additional benefit of ultra-high dose rate (UHDR) capability (Fischer *et al* 2024) which introduces the potential for synergistic normal tissue sparing from the FLASH effect (Espen *et al* 2020). The sub-second irradiation time associated with UHDR irradiations may benefit SFRT irradiations by preventing any blurring of the SFRT distribution due to patient motion during treatment. Some degree of blurring ($< 5 \text{ mm}$ in any direction) has been tolerated in clinical cases, however the clinical significance of SFRT blurring remains unknown (Grams *et al* 2023). Moreover, with energies exceeding 100 MeV, VHEEs can penetrate to depths suitable for treating deep-seated tumors, an advantage over clinically available electron beams. Penetration depth is heavily influenced by beam size, where small beamlets show reduced penetration (DesRosiers *et al* 2000).

SFRT has previously been administered for MV photon beams through a variety of techniques including a static block collimator with a grid channels or use of the multileaf collimators (Neuner *et al* 2012, Billena and Khan 2019). For charged particle sources such as protons and VHEEs, an electromagnetic field can be used to steer the beam and deliver SFRT through pencil beam spot scanning. A study on proton SFRT found that for beamlet spacings larger than 2.8 mm pencil beam scanning produced greater PVDR values compared to using a grid collimator (Prezado and Fois 2013). In a study by Clements *et al* a tungsten grid collimator was used to produce SFRT distributions on radiochromic film using the 140–200 MeV electrons (2024). Substantial Bremsstrahlung production in the tungsten collimator yielded low PVDR values (2–4) at a depth of 13 mm and shallow DOCs (39–47 mm). The sub-optimal PVDR and DOC values limit the applicability of this work to shallow tumors. Pencil beam spot scanning might be used to reduce the Bremsstrahlung contributions. Pencil beam scanning offers the added benefit of increasing achievable dose rates, a key parameter believed to be crucial for achieving the FLASH effect. In contrast, the use of a mechanical collimator can reduce dose rates, limiting its applicability to FLASH radiotherapy.

The aim of this work is to investigate SFRT implemented through pencil beam spot scanning with very high energy electrons. Film dosimetry was performed with a submillimeter pencil beam, approximately in the minibeam size range, to create a spot scanning pattern, and the resulting dose distributions were investigated based on PVDR and DOC. To further expand on the dosimetry work, MC simulations were utilized to demonstrate the idealized potential of the experimental set up and compare to experimental results. Finally, SFRT treatment plans for a canine glioma case were simulated using the MC beam model and compared to a clinical 6 MV VMAT plan.

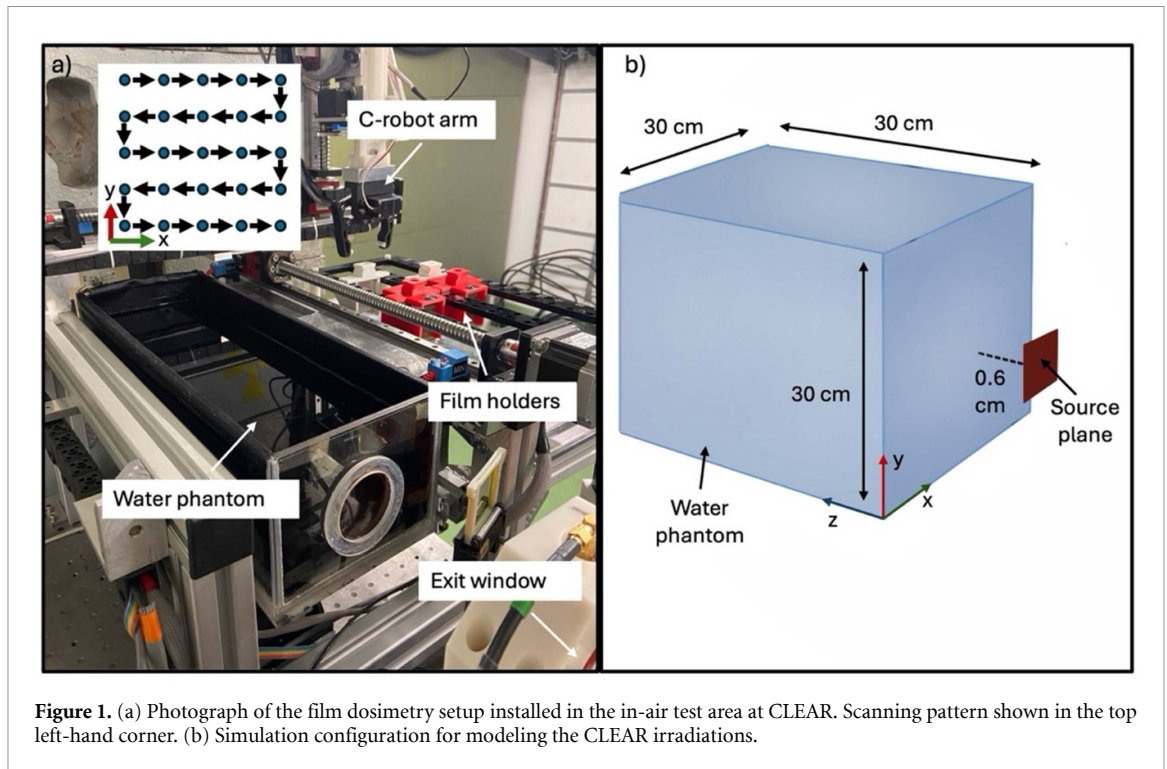


Figure 1. (a) Photograph of the film dosimetry setup installed in the in-air test area at CLEAR. Scanning pattern shown in the top left-hand corner. (b) Simulation configuration for modeling the CLEAR irradiations.

2. Materials and methods

2.1. Experimental Set-up

The measurements described in this work were conducted at the CERN linear electron accelerator for research (CLEAR) which is a user test facility capable of accelerating electrons up to 220 MeV (Korysko *et al* 2023). The CLEAR beamline time structure consists of bunches of electrons which can be up to 10 ps in length delivered at 1.5–3 GHz frequency; these bunches can be grouped into trains delivered at 0.883–10 Hz frequency which may have up to 200 bunches (Korysko *et al* 2023). The CLEAR beamline is 37 m in length and includes an in-air test area located at the end of the beamline. The in-air test area can be modified for various experimental set-ups. A polymethyl methacrylate (PMMA) water tank with a kapton window was installed and centered with the beam at a distance of 40.5 cm from the exit window (figure 1). The CLEAR-robot (C-Robot) was positioned alongside the water tank and allowed samples to be remotely moved in and out of the path of the beam. The C-Robot is made up of a 3D printed grabber positioned on linear motion stages that allow samples to be moved in along the X, Y and Z axis (Korysko *et al* 2023). A camera monitors samples and aids in their placement and a stand placed next to the water to tank stores samples between irradiations.

Custom 3D-printed film holders were designed to hold up to 14 films, each separated by 5 mm. Groups of five films, each measuring 35×40 mm, were placed within the holder at 10 mm intervals. The C-Robot positioned the film holder within the water tank so that the first film was 12 mm from the kapton window of the water tank. An additional background film was left in the stand during irradiations to measure scattered dose that film samples may have received during beam tuning or irradiation of other samples. The background dose was measured to be negligible at <0.03 Gy and was not subtracted from experimental data.

To simulate pencil beam scanning, the C-Robot maneuvered the film holder in the X and Y directions. The film holder moved in increments of 3, 4, or 5 mm, creating a 5×5 grid pattern of evenly spaced pencil beams. At each position in the 3 and 4 mm spaced grids, single bunch shots of 100 pC charge were delivered. The specific charge was selected to achieve a target peak dose of 15 Gy, ensuring the dose remained within the film's dynamic range of 0.1–20 Gy. For the 5 mm spaced grid, each shot was 200 pC. With larger grid spacing, there was potential for the valley dose to fall below the film detection threshold. To mitigate this, the charge per pulse was increased for the 5 mm spacing. An additional set of test films was utilized to obtain beam definition. This set did not have a complete 5×5 grid but instead a 2×2 grid with 12 mm spacing between pencil beams. In this grid, two shots were delivered with 100 pC and two shots were delivered with 50 pC.

2.2. Film dosimetry

GAFchromic EBT3 films (Ashland Inc., Wayne, NJ, USA) were used which have been previously established to be dose rate independent up to $8 \times 10^6 \text{ Gy s}^{-1}$ (Jaccard *et al* 2017) and energy independent up to 165 MeV. Experimental studies have yet to be conducted on the energy dependence beyond 165 MeV (Subiel *et al* 2014) and a recent MC study (Clements and Bazalova-Carter 2024) demonstrated film measurement errors of up to 2.5% for VHEEs which increases the uncertainty of the film dose. EBT3 film was ultimately selected for its well documented use in VHEE studies, dose rate independence, high spatial resolution, and dose accuracy (Sorriaux *et al* 2013, Bazalova-Carter *et al* 2015, Clements *et al* 2024). A 5.5 MeV electron beam from an eRT6 Oriatron was used to calibrate film to dose-to-water using a dose rate of 0.05 Gy s^{-1} .

The films were scanned at 300 dpi resolution 24 h following radiation exposure using an Epson Perfection V800 flatbed scanner (Suwa, Japan). Film analysis was performed using a custom Python version 3.9.6 script to calculate the net optical density and convert to dose. Green channel net optical density was calculated by taking the logarithm of the ratio between a background film and the irradiated film. Net optical density was related to dose through a curve fit modeled by the equation $\text{NetOD} = \frac{a+b*D}{D+c}$, where a , b , and c are constants determined through calibration of the film and D is the dose given to the film.

2.3. Film analysis

An in-house Python peak finding algorithm was used to identify the center of peaks on irradiated films. To determine the CLEAR VHEE pencil beam model, the peak finding algorithm was applied to the 2×2 test films. One-dimensional dose (D) profiles were drawn in the X and Y directions for each peak normalized per delivered charge. A Gaussian fit was applied to the one-dimensional profiles using the form

$$D = h + ae^{-\frac{(x-x_0)^2}{2\sigma^2}} \quad (1)$$

where a , h , x_0 and σ are fit parameters and x is the position along the profile. From the Gaussian fit, the peak dose and spread of the Gaussian were extracted. An average of the Gaussian fit parameters was assumed to represent the CLEAR beam used in further studies.

In the 2×2 test film, leakage dose was identified by observing higher dose levels along the path of movement between spots. The leakage was measured by averaging the dose values in the outermost 2.5 mm of each profile, specifically in the direction of movement.

For each SFRT distribution, the mean peak dose was calculated by identifying the peaks and taking the mean of $0.255 \times 0.255 \text{ mm}$ regions of interest (ROI) for all peaks. The uncertainty of the mean peak dose was calculated as the standard error of the ROIs. To calculate the mean valley dose, the midpoints between adjacent peaks were identified as valleys. These valley points were then connected to others within the same row or column, depending on whether they were between vertically or horizontally spaced peaks. The valley dose was measured along eight lines, each with a width of 3 pixels, 0.255 mm, spanning the length of the grid field. Following from the peak dose, the uncertainty was determined to be the standard error of the valley ROIs.

From the mean peak and mean valley values, the PVDR was calculated as

$$\text{PVDR} = \frac{\langle D_{\text{peak}} \rangle}{\langle D_{\text{valley}} \rangle} \quad (2)$$

where $\langle D_{\text{peak}} \rangle$ is the mean peak dose and $\langle D_{\text{valley}} \rangle$ is the mean valley dose. The resulting uncertainty for PVDR is given as

$$\Delta \text{PVDR} = \sqrt{\left(\frac{\Delta \langle D_{\text{peak}} \rangle}{\langle D_{\text{peak}} \rangle}\right)^2 + \left(\frac{\Delta \langle D_{\text{valley}} \rangle}{\langle D_{\text{valley}} \rangle}\right)^2} \quad (3)$$

where $\Delta \langle D_{\text{peak}} \rangle$ and $\Delta \langle D_{\text{valley}} \rangle$ are the standard error of the mean peak dose and mean valley dose, respectively. From the PVDR, the DOC was calculated as the depth where $\text{PVDR} < 1.1$. To find this depth, the PVDR values were plotted as a function of depth and the curve was extrapolated with an exponential decay fit.

2.3.1. Pencil beam Monte Carlo simulations

The irradiations performed at CERN were simulated using TOPAS MC version 3.9 (Perl *et al* 2012, Faddegon *et al* 2020), a particle simulation tool that wraps and extends GEANT4. The range cutoff was set at 0.05 mm, approximately an order of magnitude smaller than the beamlet width, to preserve the fine details of the dose distribution. Previous MC studies with VHEE have established a common set of physics lists. In this study, the following physics lists were applied: g4em-standard-opt4 and g4em-extra to accurately model electromagnetic processes; g4h-elastic_HP for elastic nuclear interactions; g4ion-binarycascade and g4h-phy_QGSP_BIC_HP for inelastic nuclear interactions. Additionally, g4decay and g4radioactivedecay

were included to model particle decay, and g4stopping was used to account for nuclear capture at rest. All other physics parameters used the default settings. MC simulations were run on a compute Canada cluster with 64 CPUs (2.40 GHz) or on a Linux computer with 16 CPUs (4.80 GHz) and took from 21 h for single pencil beam simulations to 7 d for the glioma case to complete.

The MC model consisted of a $30 \times 30 \times 30 \text{ cm}^3$ water phantom, in which the PMMA container was approximated as water. The beam was defined at 0.6 cm from the water tank and had an energy based on experimental measurements of 194.0 MeV with 2.0 MeV energy spread. The beam angular spread and position spread values were adjusted until an agreement was found between the simulation and experiments. The agreement was based on minimizing the sum of the difference in the beam σ values (equation (1)) between the film and simulation at each depth. The beam was simulated with 1×10^7 primary electrons and was determined to be symmetrical with a positional spread (σ) of 0.46 mm and an angular spread of 0.68° . The leakage dose was added to the MC results. Simulations which included the exit window, PMMA water container and yttrium aluminum garnet screen indicated that these components had negligible $<1\%$ change on the peak dose and σ of the simulated beam. For this reason, the additional components were removed from simulations.

The mean dose to water per particle and the standard deviation was scored in a $2 \times 2 \times 8 \text{ cm}^3$ section of the water phantom along the beam central axis. The scored volume consisted of $0.1 \times 0.1 \times 0.25 \text{ mm}^3$ voxels that aimed to approximate the resolution (0.085 mm) and thickness (0.28 mm) of the EBT3 film. The mean dose to water per particle was converted to mean dose by multiplying by the estimated total number of electrons delivered to the film during the irradiations. The total number of particles delivered was obtained by dividing the total experimental charge delivered by the fundamental charge.

For SFRT, twenty-five simulations of 1×10^6 primary electrons were run in parallel for each spot position in the grid; these simulations were used to reconstruct the pencil beam scanning pattern. Each of the dose distributions were superimposed onto a predefined grid to create SFRT grid patterns with 3, 4 and 5 mm spacing. The peaks and valleys of the MC simulation were evaluated using the algorithm developed for film analysis. Given the slight discrepancy in pixel size between the film and MC simulation, the peak ROIs were $0.3 \times 0.3 \text{ mm}$, and the valley ROIs were 0.3 mm wide. The peak dose, valley dose, and PVDR was compared at each depth to the film results.

2.4. Canine glioma case

Single-fraction treatment plans were developed for a canine glioma patient using computed tomography (CT) images and the MC beam model developed from the film dosimetry at CLEAR. The canine patient had a 14.1 cm^3 tumor at the back of the brain resting along the brainstem. A dose of 26.5 Gy was prescribed to the 95% of the planning target volume (PTV) and was delivered using VMAT with 6 MV photons. This VMAT treatment was delivered clinically and in this study two VHEE plans were simulated using 194 MeV SFRT and 125 MeV SFRT with 4 mm pencil beam spacing. The 4 mm step size was selected because the 5 mm step size was too large to achieve acceptable target CI. Furthermore, the tumor was not deep enough to require a 5 mm step size to maintain a high PVDR at depth, and the 4 mm step size provided sufficient PVDR in the surrounding normal tissue. Pencil beams were delivered from 5 equidistant angles in the axial plane. A research version of RayStation (version 2023B, RaySearch Laboratories AB, Stockholm, Sweden) was employed to determine the pencil beams which intersected with the tumor volume. The proton pencil beam scanning feature was utilized to select the pencil beam positions to create an optimal dose distribution (Janson *et al* 2024). Each pencil beam was simulated using 1×10^5 electrons at 85 mm source-to-axis distance. The dose was scored in the entire CT volume with $2.00 \times 0.35 \times 0.35 \text{ mm}^3$ voxels using the Schneider CT HU-to-material conversion (Uwe Schneider *et al* 1996). The dose distributions were normalized by the ratio of the dose received by 95% (D_{95}) of the PTV in the VHEE plan to that in the VMAT plan. The dose volume histograms (DVHs) and the relevant parameters describing dose to the PTV and organs at risks (OARs) was extracted for each plan. The CI and homogeneity (HI) indices were calculated with:

$$\text{CI} = \frac{V_{95\%}}{V_{\text{PTV}}} \quad (4)$$

$$\text{HI} = \frac{D_x}{D_{95}} \quad (5)$$

where V_{PTV} is the PTV volume, $V_{95\%}$ is the volume encompassed by 95% of the prescription dose, and V_x is the lowest dose received by at least $x\%$ of the PTV.

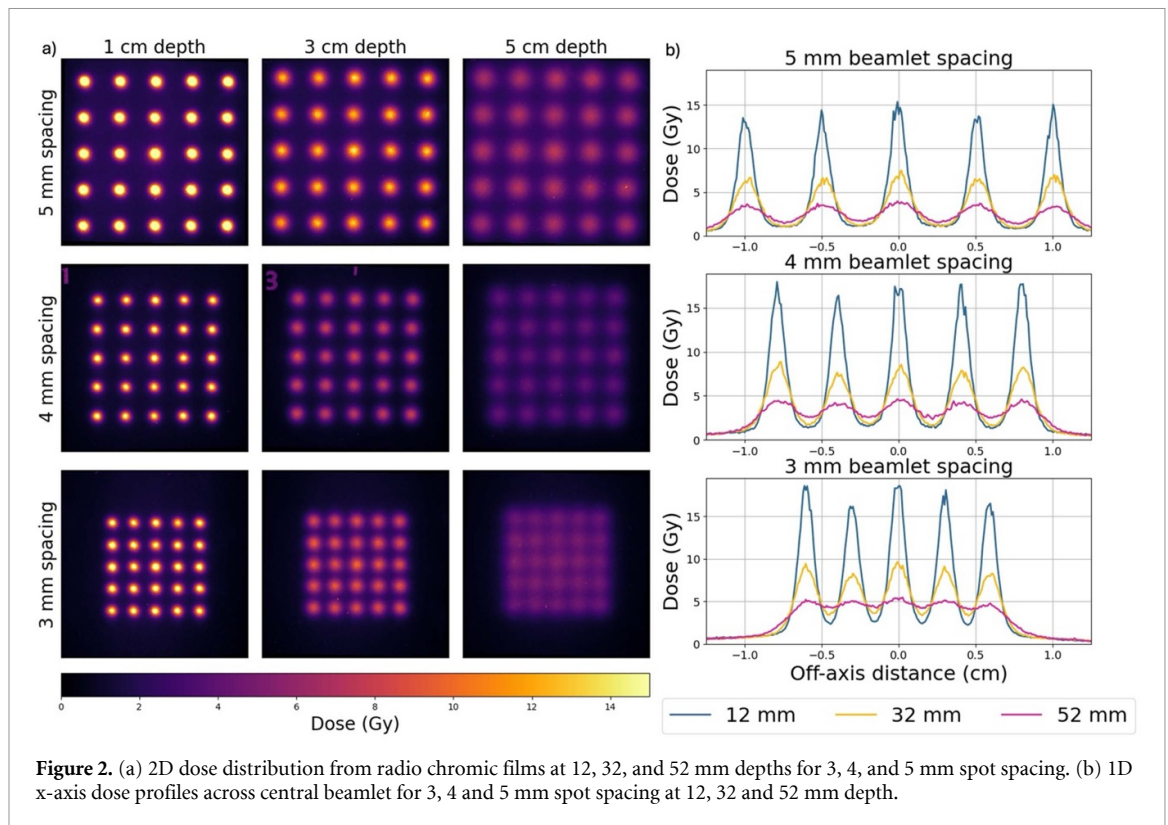


Figure 2. (a) 2D dose distribution from radio chromic films at 12, 32, and 52 mm depths for 3, 4, and 5 mm spot spacing. (b) 1D x-axis dose profiles across central beamlet for 3, 4 and 5 mm spot spacing at 12, 32 and 52 mm depth.

3. Results

3.1. Film dosimetry

Films and beam profiles for the 5, 4, and 3 mm spacings at 12, 32, and 52 mm depths are shown in figure 2. The center-to-center distance of the 3 mm spot spacing was found to be 2.98 ± 0.03 mm in the x -axis and 3.00 ± 0.04 mm in the y -axis. The spot spacing of the pencil beams was determined to be 3.98 ± 0.03 mm and 4.02 ± 0.04 mm for the 4 mm case in the x and y -axis, respectively. The 5 mm spot spacing showed similar accuracy with a mean spacing of 4.99 ± 0.03 mm in the x -axis and 5.01 ± 0.01 mm in the y -axis.

Normalized peak doses presented in figure 3(a) demonstrate very similar behavior for all three beam spacings. Due to beamlet overlap at the 5 cm depth, the 3 mm beamlet spacing dose is higher. The valley dose, shown in figure 3(b), followed similar trends across all pencil beam spot spacings. As expected, due to the same pencil beam size, the valley dose rate was highest for the 3 mm spacing while the 5 mm spacing showed the lowest valley dose. The valley dose was as high as 2.8 times (at 32 mm depth) higher with 3 mm spacing than 5 mm spacing. The valley dose as a percentage of the peak dose at 12 mm depth was $13.24 \pm 0.07\%$ with 3 mm spot spacing, $7.57 \pm 0.02\%$ with 4 mm spot spacing, and $6.46 \pm 0.02\%$ with 5 mm spot spacing. The leakage dose accounted for a significant portion of the valley dose, up to 68% for the 5 mm spacing. Leakage dose of 0.51 ± 0.05 Gy was measured at 12 mm and dropped off to 0.41 ± 0.05 Gy at 52 mm.

PVDR presented in figure 3(c) decreased with depth. The PVDRs showed the highest value of 15.5 ± 0.1 for 5 mm spot spacing. A PVDR of 13.2 ± 0.1 with 4 mm spacing and 7.5 ± 0.1 with 3 mm spacing was observed. The peaks could be distinguished at the largest recorded film depth of 52 mm and the DOC (PVDR < 1.1) was extrapolated to be 56.6, 70.7, and 76.5 mm for 3, 4, and 5 mm spot spacing, respectively.

3.2. Pencil beam Monte Carlo simulations

Figure 4(a) shows the experimental and simulated MC percent depth dose curves for the 194 MeV VHEE beam. There is good agreement with a maximum dose difference of 2% between MC simulations and film results. Figure 4(b) compares the simulated and experimental beam sizes as a function of depth. The difference in profile, measured by σ_x and σ_y , was less than 3% between MC simulations and film measurements.

To compare the simulated and experimental results, the MC simulations were adjusted by including the leakage dose that was measured on the film, as this leakage dose could not be accurately simulated. In figure 5, MC results without leakage dose are compared to the experimental results at 12 mm (a), 32 mm (b), and 52 mm (c) depth. The additional leakage dose contributes to increasing the peak dose but also increases the valley dose. The increase in valley dose is a limiting factor for achieving high PVDR values. The MC

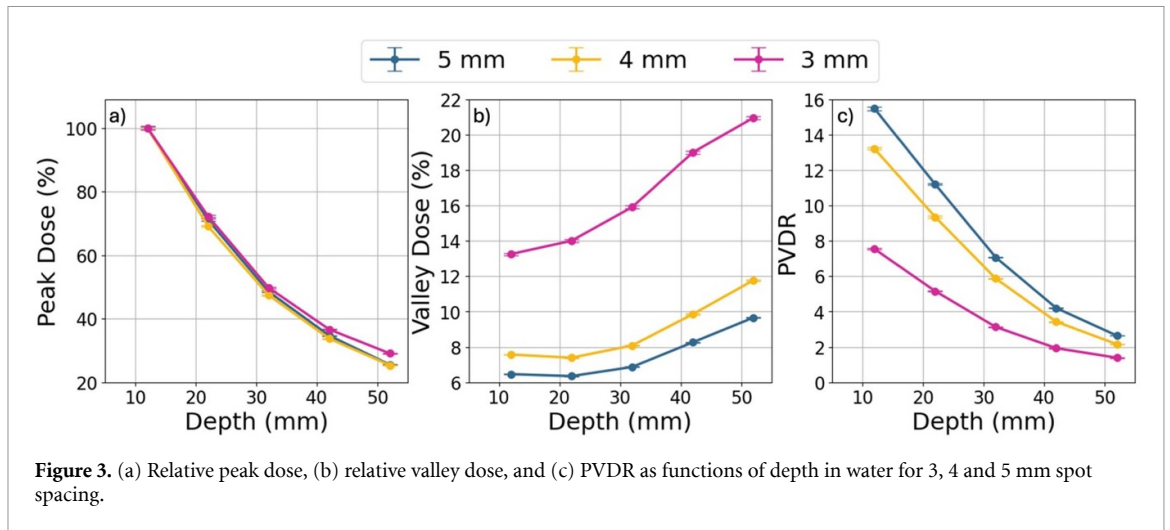


Figure 3. (a) Relative peak dose, (b) relative valley dose, and (c) PVDR as functions of depth in water for 3, 4 and 5 mm spot spacing.

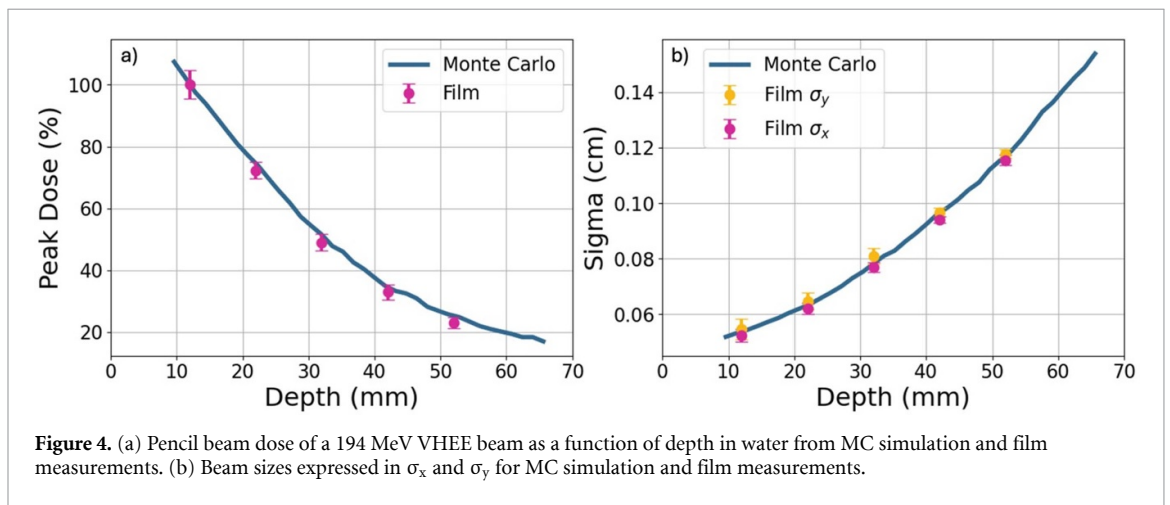


Figure 4. (a) Pencil beam dose of a 194 MeV VHEE beam as a function of depth in water from MC simulation and film measurements. (b) Beam sizes expressed in σ_x and σ_y for MC simulation and film measurements.

results without leakage, presented in figure 5, demonstrate the achievable PVDR values if the contribution of the leakage dose were mitigated. In MC simulations, the valley dose ranged from 0.5% to 16% of the peak dose at 12 mm depth. As shown in figure 5(d), the relative dose in the valleys maintains a similar trend to the experimental results presented in figure 3(b).

The significantly lower valley doses in the MC simulations lead to far greater PVDR values, as shown in figure 5(e). The greatest PVDR achieved at 12 mm depth for 5 mm spot spacing was 180 ± 4 . The PVDR at 12 mm was 115 ± 3 for 4 mm spot spacing and it was 19 ± 1 for 3 mm spot spacing. The PVDR values decreased with depth but showed a steeper decline with depth compared to the experimentally obtained values. The PVDR values at shallow depths were much greater, but due to the sharp fall-off, the DOC was lower. The DOC was found to be 69.9, 65.4, and 53.2 mm for 5, 4, and 3 mm spot spacing, respectively.

3.3. Canine glioma treatment simulations

The canine glioma dose distributions, DVHs, and mean OAR doses for the clinically delivered 6 MV VMAT plan, the 194 MeV VHEE SFRT plan and the 125 MeV VHEE SFRT plan are presented in figure 6. The prescription dose was 26.5 Gy prescribed to the 95% of the PTV delivered using 4 mm spaced pencil beams. The mean doses for both VHEE treatments showed improved metrics compared to the VMAT plans with lower doses to OAR while delivering greater mean dose to the PTV.

All OARs received lower mean doses in both the VHEE SFRT plans compared to the VMAT plan, with maximum OAR sparing for the left ear in the 194 MeV case (59%) and right ear, spinal cord, and brain-PTV lowering the mean dose by at least 16%. Furthermore, due to spatial fractionation creating hot spots, the dose to the PTV was increased by 15% in the 194 MeV plan. The mean dose to OAR showed minimal variation between the 194 and 125 MeV plans with the greatest difference shown in the left ear which had 4% greater mean dose in the 125 MeV plan. The mean dose to the PTV varied by 0.5% between VHEE plans. Furthermore, the mean dose to the left and right eyes was reduced from 0.22 Gy to less than 0.001 Gy in both VHEE plans.

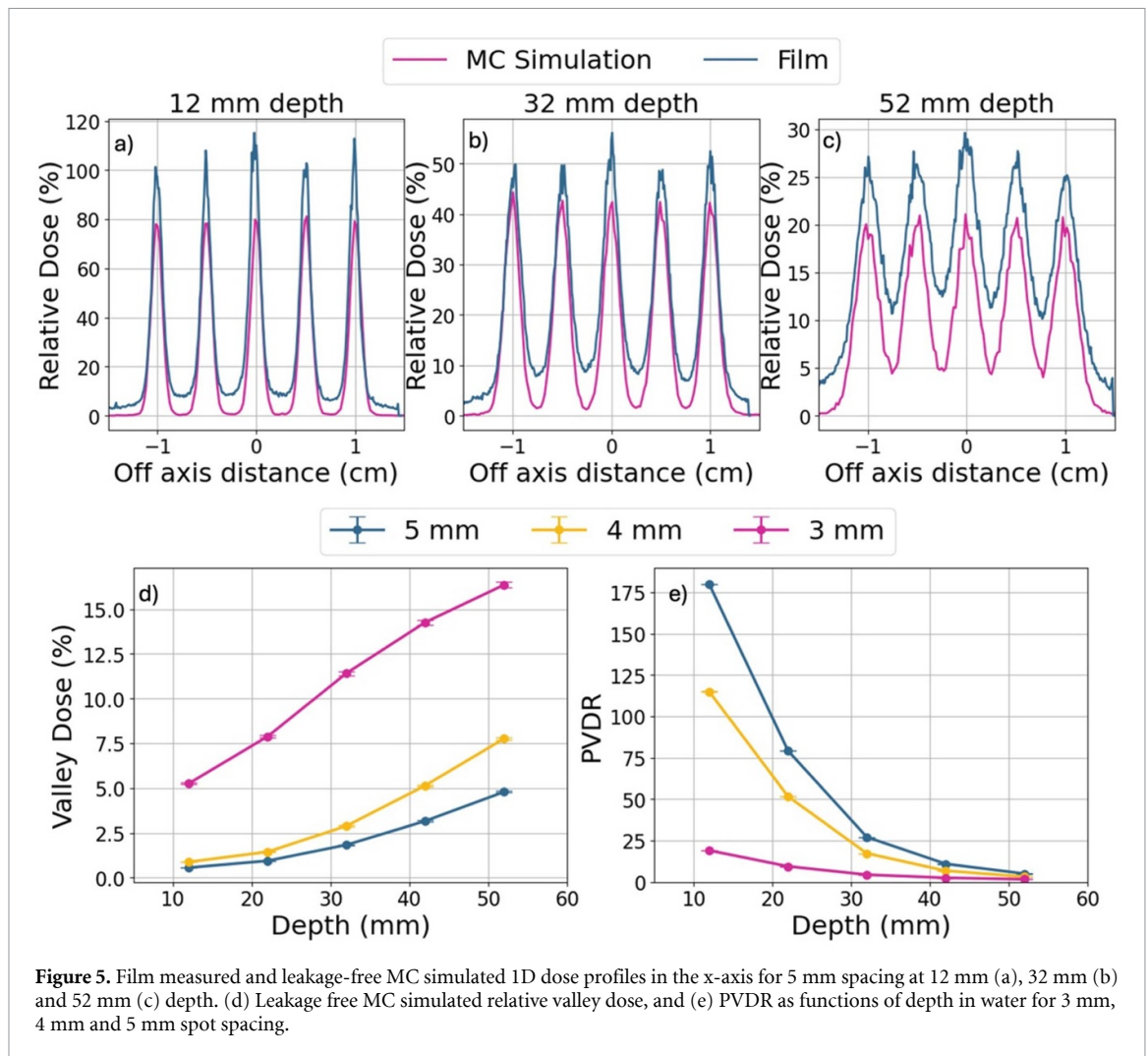


Figure 5. Film measured and leakage-free MC simulated 1D dose profiles in the x-axis for 5 mm spacing at 12 mm (a), 32 mm (b) and 52 mm (c) depth. (d) Leakage free MC simulated relative valley dose, and (e) PVDR as functions of depth in water for 3 mm, 4 mm and 5 mm spot spacing.

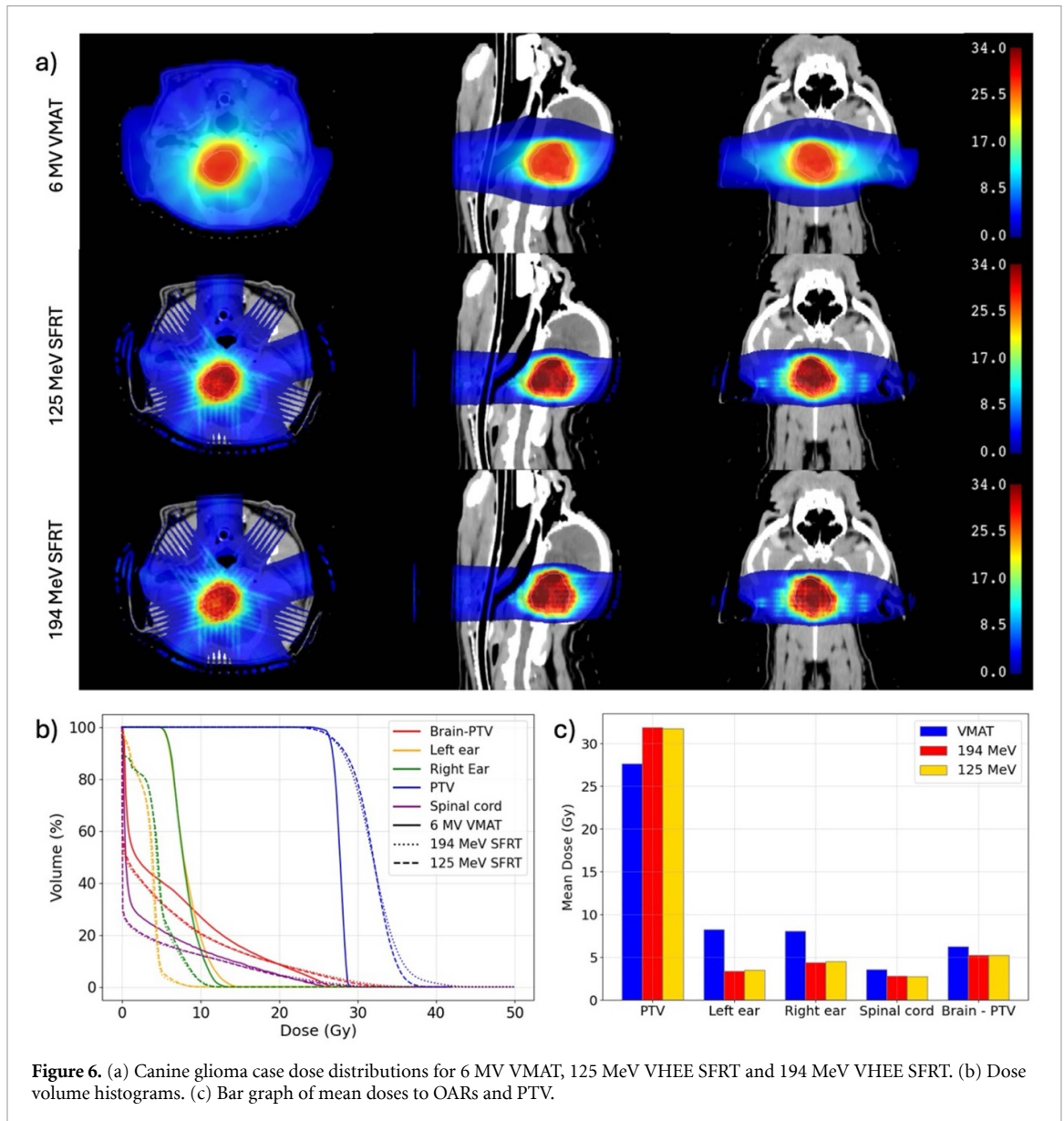
The SFRT delivery of the VHEE plan resulted in hotspots within the PTV. A maximum dose of 40 Gy in the 125 MeV plan and 46 Gy in the 194 MeV plan was found within the PTV compared with 29 Gy for the VMAT plan. The characteristic inhomogeneity associated with SFRT is reflected in the homogeneity index, which was 1.31, 1.37 and 1.08 for the 125 MeV VHEE SFRT, 194 MeV VHEE SFRT and 6 MV VMAT plans respectively. The maximum dose increased by 21% in the spinal cord and by 39% in the brain-PTV for the 125 MeV VHEE SFRT plan compared to the VMAT plan. The 194 MeV VHEE SFRT plan showed poorer results with the brain-PTV receiving a maximum dose which was 57% higher than the clinical plan. The 125 MeV VHEE SFRT plan, with a CI of 0.95, demonstrated better CI compared to the VMAT plan, which had a CI of 0.85. Similarly, the 194 MeV VHEE SFRT plan achieved comparable results with a CI of 0.94. The surface PVDR was 885 ± 3 for 125 MeV and 894 ± 3 for 194 MeV. The DOC decreased to 53.1 mm for 125 MeV compared to 65.4 mm for 194 MeV.

4. Discussion

This study investigated SFRT delivered with a VHEE source, a technique which could maximize normal tissue sparing in combination with ultrahigh dose-rate delivery potentially resulting in the FLASH effect. The physical properties of VHEEs, including their reduced lateral scatter, and relative insensitivity to tissue inhomogeneities, offer a unique opportunity to achieve optimal dosimetric parameters for SFRT, even in deep-seated tumors. In this study radio chromic films were irradiated using a step-and-shoot method to create VHEE SFRT dose distribution.

4.1. Film dosimetry and Monte Carlo simulations

Experimental dose distribution demonstrated higher PVDRs (<15.5) and greater depths of convergence (76.5 mm) compared to previous work which investigated VHEE SFRT delivered with a tungsten grid collimator. Using the tungsten grid collimator, PVDRs of 2–4 at 13 mm depth and DOC up to 47 mm were



observed (Clements *et al* 2024). The improved SFRT dose metrics found in this study could allow for the treatment of many deep-seated tumor such as head and neck cancers or lung tumors. Furthermore, pencil beam scanning could reduce the limitation of the small field currently associated with VHEE accelerators. Electromagnetic pencil beam scanning may be used to deflect the beam from its original path and reach the edge of a larger field.

Minimizing the center-to-center spot distance has been related to sparing healthy tissue and it has been observed that larger $c-t-c$ in relation to the beam size may eliminate the sparing associated with SFRT (Datzmann *et al* 2020, Ahmed *et al* 2023). However, for the same beam size a lower $c-t-c$ may increase valley dose and decrease PVDRs as the gaussian beam shape and scatter cause the spots to blur into one another. As seen in the 3 mm spot spacing, the valley dose was nearly 3 times higher than the 5 mm spot spacing.

The accuracy of the MC simulations of the experimental setup was constrained by several factors that may have contributed to the discrepancies observed when compared with the measurements. Absolute dose differences between MC simulations calculated based on the delivered charge and film measurements were between 17% and 25%, and the dose difference decreased with depth. This may be partially attributed to inaccurate charge measurements and to photon dose which is not accurately captured on the radiochromic films that were calibrated with 5.5 MeV electrons. It has been shown that for the same delivered dose electrons create a lower optical density response in EBT3 films compared to photons (Sorriaux *et al* 2013). Bremsstrahlung production in the water was evaluated in secondary simulations and found to be increasing with depth up to 20% of the total dose at 60 mm depth. Despite the discrepancies in absolute dose, the relative dose MC simulations showed good agreement with the experimental results. The maximum

differences in the relative peak dose were observed to be 2% and the difference in the beam profile measured by σ_x and σ_y was 3%.

The 2×2 test film revealed a leakage dose along the scanning pattern's path. This dose could not be attributed to scatter, as it was not uniformly distributed around each pencil beam spot. Instead, the additional dose is likely due to charge leakage in the beamline caused by dark current. The dark current of CLEAR beamline is estimated to be approximately 1 pC per pulse and is generated with a 10 Hz repetition rate.

Although the precise dose rate was not measured for this work, VHEE sources are generally considered to be UHDR capable which presents the opportunity for potential synergistic normal tissue sparing between SFRT and FLASH. Previous work done on the CLEAR beamline has shown the instantaneous peak dose rates to be on the order of 10^8 Gy s⁻¹ or greater (Clements *et al* 2024, Hart *et al* 2024). Given that each spot was delivered in a single bunch, it can be estimated that the instantaneous dose rate was similar to previous experiments. Dose rates produced on the CLEAR beamline are well above those that have been shown to produce the FLASH effect (Montay-Gruel *et al* 2017, 2021).

4.2. Canine glioma case

A canine glioma case was selected to demonstrate a treatment plan as a canine patient features tumors at a depth suitable to the calculated PVDRs. The treatment plan presented in figure 6 was designed with five static beams which allowed the VHEE treatments to completely avoid key critical organs like the eyes which received zero dose and the bulk of the brain stem. The low dose bath in the VMAT plan extended towards the eyes of the patient and encompassed a greater portion of the spinal cord. The mean doses delivered by the VHEE plans demonstrated greater dose to the PTV and lower doses to the OARs.

The 125 and 194 MeV VHEE SFRT plans vary by a maximum of 4% in mean dose to the OARs and there is no difference in mean dose to the PTV. However, the 125 and 194 MeV plans vary significantly in terms of maximum dose to OARs. The 194 MeV plan delivered 12% and 4% greater maximum dose to the brain-PTV and spinal cord, respectively compared to the VMAT plan. This may be in part due to the normalization scheme which normalized the VHEE plans by the dose received by 95% of the PTV. The more homogeneous distribution presented by the 125 MeV case resulted in a greater dose covering 95% of the PTV and allowed the dose to the surrounding tissue to be decreased.

The canine case VHEE SFRT dose distributions show various levels of PTV dose homogeneity. By decreasing the beam energy from 194 to 125 MeV, the DOC was decreased from 65.4 to 53.1 mm which allowed for a more homogeneous dose within the tumor. The presented work demonstrates how converging beams with strategic DOC may be used to yield a dose distribution with non-uniform dose within the normal tissue and a more uniform coverage within the tumor. The non-uniformity in the target could be improved by using beam weighting. This study demonstrated a simplified treatment in which 5 beam angles are used to treat the tumor volume using pencil beam scanning. Beam and beamlet weighting that was kept uniform could further improve the CI of the dose distribution and reduce the dose to OARs. Recent SFRT studies have shown that local tumor control can be achieved without completely homogeneous dose in the PTV, thus the inclusion of beam weighting should mainly be used to improve CI (Prezado *et al* 2018, Lansonneur *et al* 2020). In fact, hot spots within the tumor volume are common in radiosurgery and interstitial brachytherapy treatments. According to a fundamental principle of radiotherapy, higher doses to the tumor are expected to increase tumor control probability (Tomé and Fowler 2000). As a result, there has been interest in techniques to escalate the dose within the tumor (Hrinivich *et al* 2019).

However, the location of the tumor may make it difficult to completely spare these critical organs. The clinically delivered VMAT plan was also shown to exceed the recommend dose limits for both the spinal cord and the brain-PTV (Trageser *et al* 2023). Delivering this treatment using both FLASH and SFRT could relieve some damage to the surrounding normal tissue. Previous studies investigating FLASH treatment plans have considered the use of a 'dose modifying factor' to account for the normal tissue sparing effects of the FLASH effect. The sparing effect has been considered to be as large as 40% (Bourhis *et al* 2019, Sarti *et al* 2021, Rothwell *et al* 2022). Furthermore, this line of thought would imply an additional modifying factor associated with SFRT serving to further widen the therapeutic window.

5. Conclusion

A step-and-shoot spatially fractionated dose distribution was delivered with a 194 MeV very high-energy electron pencil beams at the CLEAR user facility at CERN. Irradiations were performed for 3, 4 and 5 mm spot spacing and later replicated in MC simulation. Experimental PVDRs of up to 15.5 ± 0.1 and depths of convergence up to 76.5 mm were achieved. Monte Carlo simulations demonstrated that reducing leakage dose could increase the PVDRs to values as high as 180 ± 4 , although the increase in PVDR did not increase the DOC as the fall off was sharper. Our results show that VHEE SFRT treatments may be suitable for specific

deep-seated tumors. To demonstrate the application of VHEE SFRT, a canine glioma treatment plan was developed for 125 and 194 MeV VHEE SFRT. The VHEE plans presented lower mean doses to OARs and greater mean dose to the PTV compared to the 6 MV VMAT plan. The maximum dose to serial organs such as the spinal cord presented a challenge as the lack of CI in the VHEE plans caused dose spill around the margins of the PTV. Further optimization including beamlet weighting, evaluation of beam angle and number of beams could improve the plan metrics such as CI and reduce dose to critical structures.









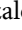
Data availability statement

The data cannot be made publicly available upon publication because they are not available in a format that is sufficiently accessible or reusable by other researchers. The data that support the findings of this study are available upon reasonable request from the authors.

Acknowledgment

The authors would like to acknowledge funding from NSERC Discovery Grants and the Canada Research Chairs program. Additionally, support from the Digital Research Alliance of Canada was instrumental in facilitating this research. Additionally, the authors would like to acknowledge RaySearch for providing us with a license to a research version of RayStation.

ORCID iDs

Jade Fischer  <https://orcid.org/0009-0000-8862-1263>
Alexander Hart  <https://orcid.org/0000-0002-0547-5887>
Nicole Bedriová  <https://orcid.org/0009-0003-0851-6810>
Deae-eddine Krim  <https://orcid.org/0009-0000-1504-598X>
Nathan Clements  <https://orcid.org/0000-0001-8911-997X>
Joseph Bateman  <https://orcid.org/0000-0002-5967-6748>
Pierre Korysko  <https://orcid.org/0000-0002-7878-2298>
Manjit Dosanjh  <https://orcid.org/0000-0003-1378-349X>
Magdalena Bazalova-Carter  <https://orcid.org/0000-0002-9365-2889>

References

- Ahmed M, Bicher S, Stewart R D, Bartzsch S, Schmid T E, Combs S E and Meyer J 2023 Dosimetric quantities and cell survival for spatially fractionated radiation therapy *Front. Phys.* **10** 1064860
- Ahmed S K, Petersen I A, Grams M P, Finley R R, Haddock M G and Owen D 2024 Spatially fractionated radiation therapy in sarcomas: a large single-institution experience *Adv. Radiat. Oncol.* **9** 101401
- Anderson D, Siegbahn E A, Fallone B G, Serduc R and Warkentin B 2012 Evaluation of dose-volume metrics for microbeam radiation therapy dose distributions in head phantoms of various sizes using Monte Carlo simulations *Phys. Med. Biol.* **57** 3223–48
- Asur R, Butterworth K T, Penagaricano J A, Prise K M and Griffin R J 2015 High dose bystander effects in spatially fractionated radiation therapy *Cancer Lett.* **356** 52–57
- Bazalova-Carter M *et al* 2015 Comparison of film measurements and Monte Carlo simulations of dose delivered with very high-energy electron beams in a polystyrene phantom *Med. Phys.* **42** 1606–13
- Billena C and Khan A J 2019 A current review of spatial fractionation: back to the future? *Int. J. Radiat. Oncol. Biol. Phys.* **104** 177–87
- Bourhis J *et al* 2019 Clinical translation of FLASH radiotherapy: why and how? *Radiother. Oncol.* **139** 11–17
- Choi J I, Daniels J, Cohen D, Li Y, Ha C S and Eng T Y 2019 Clinical outcomes of spatially fractionated GRID radiotherapy in the treatment of bulky tumors of the head and neck *Cureus* **11** e4637
- Clements N and Bazalova-Carter M 2024 Absorbed-dose energy dependence of EBT3 and EBT4 films for 5–200 MeV electrons and 100 keV–15 MeV photons *JACMP accepted*
- Clements N, Esplen N M, Bateman J J, Robertson C, Dosanjh M, Korysko P, Farabolini W, Corsini R and Bazalova-Carter M 2024 Mini-GRID radiotherapy on the CLEAR very-high-energy electron beamline: collimator optimization, film dosimetry, and Monte Carlo simulations *Phys. Med. Biol.* **69** 055003
- Clements N, Esplen N and Bazalova-Carter M 2023 A feasibility study of ultra-high dose rate mini-GRID therapy using very-high-energy electron beams for a simulated pediatric brain case *Phys. Med.* **112** 102637
- Datzmann G, Sammer M, Girst S, Mayerhofer M, Dollinger G and Reindl J 2020 Preclinical challenges in proton minibeam radiotherapy: physics and biomedical aspects *Front. Phys.* **8** 568206
- Delaney G, Jacob S, Featherstone C and Barton M 2005 The role of radiotherapy in cancer treatment: estimating optimal utilization from a review of evidence-based clinical guidelines *Cancer* **104** 1129–37
- DesRosiers C, Moskvina V, Bielajew A and Papiez L 2000 150–250 MeV electron beams in radiation therapy *Phys. Med. Biol.* **45** 1781
- Esplen N, Mendonca M S and Bazalova-Carter M 2020 Physics and biology of ultrahigh dose-rate (FLASH) radiotherapy: a topical review *Phys. Med. Biol.* **65** 23TR03
- Faddegon B, Ramos-Méndez J, Schuemann J, McNamara A, Shin J, Perl J and Paganetti H 2020 The TOPAS tool for particle simulation, a Monte Carlo simulation tool for physics, biology and clinical research *Phys. Med.* **72** 114–21
- Fernandez-Palomo C, Chang S and Prezado Y 2022 Should peak dose be used to prescribe spatially fractionated radiation therapy?—A review of preclinical studies *Cancers* **14** 3625

- Fischer J, Whitmore L, Desrosiers C, Sheehy S and Bazalova-Carter M 2024 Very high-energy electrons as radiotherapy opportunity *Eur. Phys. J. Plus* **139** 728
- Fukunaga H, Butterworth K T, McMahon S J and Prise K M 2021 A brief overview of the preclinical and clinical radiobiology of microbeam radiotherapy *Clin. Oncol.* **33** 705–12
- Gholami S, Nedaie H A, Longo F, Ay M R, Wright S and Meigooni A S 2016 Is grid therapy useful for all tumors and every grid block design? *J. Appl. Clin. Med. Phys.* **17** 206–19
- Grams M P et al 2023 Clinical aspects of spatially fractionated radiation therapy treatments *Phys. Med.* **111** 102616
- Hart A et al 2024 Plastic scintillator dosimetry of ultrahigh dose-rate 200 MeV electrons at CLEAR *IEEE Sens. J.* **24** 14229–37
- Hrinivich W T, McNutt T R and Meyer J J 2019 Radiation treatment planning with embedded dose escalation *Radiat. Oncol.* **14** 1–11
- Jaccard M, Petersson K, Buchillier T, Germond J F, Durán M T, Vozenin M C, Bourhis J, Bochud F O and Bailat C 2017 High dose-per-pulse electron beam dosimetry: usability and dose-rate independence of EBT3 Gafchromic films: usability *Med. Phys.* **44** 725–35
- Janson M, Glimelius L, Fredriksson A, Traneus E and Engwall E 2024 Treatment planning of scanned proton beams in RayStation *Med. Dosim.* **49** 2–12
- Kiseleva V, Gordon K, Vishnyakova P, Gantsova E, Elchaninov A and Fatkhudinov T 2022 Particle therapy: clinical applications and biological effects *Life* **12** 2071
- Korysko P, Dosaanjh M, Bateman J, Robertson C, Corsini R, Farabolini W, Aksoy A, Malyzhenkov A, Rieker V and Sjobak K (CLEAR) 2023 The clear user facility: a review of the experimental methods and future plans *14th Int. Particle Accelerator Conf. (Venice, Italy)* (<https://doi.org/10.18429/JACoW-IPAC2023-MOPL141>)
- Lagda A, Angal-Kalinin D, Jones J, Aitkenhead A, Kirkby K J, MacKay R, Van Herk M, Farabolini W, Zeeshan S and Jones R M 2020 Influence of heterogeneous media on very high energy electron (VHEE) dose penetration and a Monte Carlo-based comparison with existing radiotherapy modalities *Nucl. Instrum. Methods Phys. Res. B* **482** 70–81
- Lansonneur P, Mammari H, Nauraye C, Patriarca A, Hierro E, Dendale R, Prezado Y and De Marzi L 2020 First proton minibeam radiation therapy treatment plan evaluation *Sci. Rep.* **10** 7025
- Mohiuddin M, Fujita M, Regine W F, Megooni A S, Ibbott G S and Ahmed M M 1999 High-dose spatially-fractionated radiation (GRID): a new paradigm in the management of advanced cancers *Int. J. Radiat. Oncol. Biol. Phys.* **45** 721–7
- Montay-Gruel P et al 2017 Irradiation in a flash: unique sparing of memory in mice after whole brain irradiation with dose rates above 100 Gy/s *Radiother. Oncol.* **124** 365–9
- Montay-Gruel P et al 2021 Hypofractionated FLASH-RT as an effective treatment against glioblastoma that reduces neurocognitive side effects in mice *Clin. Cancer Res.* **27** 775–84
- Neuner G, Mohiuddin M M, Vander Walde N, Goloubeva O, Ha J, Yu C X and Regine W F 2012 High-dose spatially fractionated GRID radiation therapy (SFGRT): a comparison of treatment outcomes with Cerrobend vs. MLC SFGRT *Int. J. Radiat. Oncol. Biol. Phys.* **82** 1642–9
- Otto K 2008 Volumetric modulated arc therapy: IMRT in a single gantry arc *Med. Phys.* **35** 310–7
- Peñagaricano J A, Griffin R, Corry P, Moros E, Yan Y and Ratanatharathorn V 2009 Spatially fractionated (GRID) therapy for large and bulky tumors *J. Ark Med. Soc.* **105** 263–5
- Perl J, Shin J, Schümann J, Faddegon B and Paganetti H 2012 TOPAS: an innovative proton Monte Carlo platform for research and clinical applications *Med. Phys.* **39** 6818–37
- Prezado Y et al 2017 Proton minibeam radiation therapy spares normal rat brain: long-term clinical, radiological and histopathological analysis *Sci. Rep.* **7** 14403
- Prezado Y et al 2018 Proton minibeam radiation therapy widens the therapeutic index for high-grade gliomas *Sci. Rep.* **8** 16479
- Prezado Y and Fois G R 2013 Proton-minibeam radiation therapy: a proof of concept *Med. Phys.* **40** 31712
- Rivera J N, Kierski T M, Kasoji S K, Abrantes A S, Dayton P A and Chang S X 2020 Conventional dose rate spatially-fractionated radiation therapy (SFRT) treatment response and its association with dosimetric parameters-A preclinical study in a Fischer 344 rat model *PLoS One* **15** e0229053
- Rothwell B, Lowe M, Traneus E, Krieger M and Schuemann J 2022 Treatment planning considerations for the development of FLASH proton therapy *Radiother. Oncol.* **175** 222–30
- Sarti A et al 2021 Deep seated tumor treatments with electrons of high energy delivered at FLASH rates: the example of prostate cancer *Front. Oncol.* **11** 777852
- Schneider U, Pedroni E and Lomax A 1996 The calibration of CT Hounsfield units for radiotherapy treatment planning *Phys. Med. Biol.* **41** 111
- Slatkin D N, Spanne P, Dilmanian F A and Sandbora M 1992 Microbeam radiation therapy *Med. Phys.* **19** 1395–400
- Smyth L M L, Senthil S, Crosbie J C and Rogers P A W 2016 The normal tissue effects of microbeam radiotherapy: what do we know, and what do we need to know to plan a human clinical trial? *Int. J. Radiat. Biol.* **92** 302–11
- Snider J W et al 2020 Spatially fractionated radiotherapy (GRID) prior to standard neoadjuvant conventionally fractionated radiotherapy for bulky, high-risk soft tissue and osteosarcomas: feasibility, safety, and promising pathologic response rates *Radiat. Res.* **194** 707–14
- Sorriaux J, Kacperek A, Rossomme S, Lee J A, Bertrand D, Vynckier S and Sterpin E 2013 Evaluation of Gafchromic® EBT3 films characteristics in therapy photon, electron and proton beams *Phys. Med.* **29** 599–606
- Subiel A et al 2014 Dosimetry of very high energy electrons (VHEE) for radiotherapy applications: using radiochromic film measurements and Monte Carlo simulations *Phys. Med. Biol.* **59** 5811–29
- Tomé W A and Fowler J F 2000 Selective Boosting of Tumor Subvolumes *Int. J. Radiat. Oncol. Biol. Phys.* **48** 593599
- Trageser E, Martin T, Burdekin B, Hart C, Leary D, LaRue S and Boss M K 2023 Efficacy of stereotactic radiation therapy for the treatment of confirmed or presumed canine glioma *Vet. Comp. Oncol.* **21** 578–86
- Tubin S, Popper H H and Brcic L 2019 Novel stereotactic body radiation therapy (SBRT)-based partial tumor irradiation targeting hypoxic segment of bulky tumors (SBRT-PATHY): improvement of the radiotherapy outcome by exploiting the bystander and abscopal effects *Radiat. Oncol.* **14** 21
- Yan W et al 2020 Spatially fractionated radiation therapy: history, present and the future *Clin. Transl. Radiat. Oncol.* **20** 30–38